IETE Journal of Research

ISSN: 0377-2063 (Print) 0974-780X (Online) Journal homepage: www.tandfonline.com/journals/tijr20

A Generalized Henon Map-Based Solar PV Array Reconfiguration Technique for Power Augmentation and Mismatch Mitigation

Rayappa David Amar Raj & Kanasottu Anil Naik

To cite this article: Rayappa David Amar Raj & Kanasottu Anil Naik (2023) A Generalized Henon Map-Based Solar PV Array Reconfiguration Technique for Power Augmentation and Mismatch Mitigation, IETE Journal of Research, 69:11, 8404-8422, DOI: 10.1080/03772063.2022.2055660

To link to this article: https://doi.org/10.1080/03772063.2022.2055660

Published online: 31 Mar 2022.

IETE JOURNAL OF RESEARCH
2023, VOL. 69, NO. 11, 8404–8422
https://doi.org/10.1080/03772063.2022.2055660

A Generalized Henon Map-Based Solar PV Array Reconfiguration Technique for Power Augmentation and Mismatch Mitigation

Rayappa David Amar Raj and Kanasottu Anil Naik

Department of Electrical Engineering, National Institute of Technology, Warangal-506004, Telangana, India

ABSTRACT

The conventional PV array configurations fail to eliminate the ill effects of partial shading (PS) thereby resulting in mismatch losses. PV array reconfiguration is considered as the most competent solution for shading-related issues. However, many reconfiguration techniques reported in the literature fail to disperse the shade effectively, not compatible with large-scale arrays, and are not generalized for all array sizes. To overcome these limitations, a highly efficient generalized Henon Map technique which is extensively used in the image encryption process is proposed in this paper to reconfigure the PV array. The proposed technique is extensively analyzed for 9×9, 8×8, 4×4, 3×5 and 4×3 PV arrays under distinct shading patterns with seven parameters. The obtained results are compared with conventional Series-Parallel, Total-Cross-Tied, and very recently reported Odd-Even, Odd-Even-Prime, Chaotic Baker's Map, Magic square, and Diagonal-TCT reconfiguration techniques. Besides, an experimental prototype model is developed and tested under artificially shading conditions to validate the competence of the proposed configuration. From the comprehensive analysis, it is noted that the proposed technique offers consistently superior performance with the least percentage mismatch and maximum power enhancement of 24.17%, 25.65%, and 47.81% for various shading cases of 9×9, 8×8, and 4×4 PV arrays, respectively. Further, a qualitative comparative assessment of the proposed technique with other state-of-art techniques is presented.

KEYWORDS

Henon map; Mismatch; Partial shading; PV array; Reconfiguration; Shade dispersal

1. INTRODUCTION

Photovoltaic (PV) power generation is preferred over other renewable technologies due to its diverse advantages. However, the PV array which generates power is subjected to regularly occurring and irresistible phenomenon known as Partial Shading (PS), which is caused due to long building, trees, bird-droppings, soil, dust and snow accumulation, *etc*. [1]. The shading of PV modules in an array leads to the development of hotspots which further prompts serious fire hazards [2]. To protect the modules from hotspot heating, bypass diodes are incorporated in parallel to the modules. These diodes bypass the current under low-irradiation or PS conditions safeguarding the panel preventing from large current concentrations. Nevertheless, employing these diodes stimulates multiple power peaks (MPPs) in the characteristics of the PV array [3,4]. Further, the power obtained by the module is also lost due to bypassing of panels and thus leading to lower output.

Maximum Power Point Tracking (MPPT) systems are considered to be the possible solution for PS. A comprehensive review on conventional, hybrid, and recent soft computing MPPT-based algorithms for tracking global maximum power (GMP) has been reviewed in [5]. The commonly used MPPT algorithms are perturb and observe (P&O), hill climbing (HC), incremental conductance (INC), *etc*. [5]. Despite their effective performance in tracking the maximum power of the array, installing these controllers is a complex task and not economically feasible. Further, many of the classical MPPT techniques fail to track the

GMP under shading conditions and hence require costly and sophisticated MPPT controllers, which is not a viable solution. The improved version of the P&O MPPT approach that divides the P-V characteristics into four operating regions based on the estimation of the open-circuit voltage method is proposed to enhance the tracking speed of the PV system in [6]. A new biological-inspired squirrel search optimization algorithm-based global MPPT strategy with fast convergence and lesser power oscillations is proposed in [7]. Recently, a novel three-stage current-mode MPPT strategy with fixed and variable current-perturbation steps [8] has been proposed to enhance its performance and robustness. Employing a voltage scanning-based MPPT strategy tracks the GMP using low-level and simple microprocessors within a short time under complex shading conditions [9]. However, MPPT systems, despite

Table 1: Literature review of various static and dynamic reconfiguration techniques

Author, year	Reconfiguration Technique	Type	Array size	Remarks	Limitations/shortcomings
Parlak [11], 2014	Electrical Array Reconfiguration (EAR)	Dynamic	3×4	Employs a fixed and adaptive part, controllers, switches and switching matrix for reconfiguration	Not feasible for larger PV array sizes Increased system complexity due to huge number of switches and sensors
Deshkar [12], 2015	Genetic algorithm (GA)	Dynamic, Metaheuristic	9×9	Tested under short wide, short narrow, long narrow shading cases	Involve large computations, problems related to convergence, necessitate large search space and the selection of tuning parameters is a difficult task. All these strategies use a weighted sum approach in solving it as a multi-objective optimization problem. Choosing optimal weights is quite challenging and the selection of improper weights may result in sub-optimal output
Babu [13], 2018	Particle Swarm Optimization (PSO)	Dynamic, Metaheuristic	9×9	Reconfiguring the panels by modifying the electrical circuitry	
Yousri [14], 2020	Grey Wolf Optimization (GWO)	Dynamic, Metaheuristic	9×9	Finds the optimal structure for switching matrix for reconfiguration	
Yousri [15], 2020	Modified Harris Hawks Optimizer	Dynamic, Metaheuristic	9×9, 6×4, 6×20	Finds the optimal structure for switching matrix for reconfiguration	
Pachauri [16], 2019	Arduino-based	Dynamic	3×3	Electrical circuitry is changed by Arduino based-relay control strategy	Practical feasibility issues with large-rated systems, cost-ineffective solution for PS
Varma [17], 2021	MMTES algorithm	Dynamic	3×3, 3×4	Reconfiguration using maximum–minimum tier equalization swapping algorithm	Algorithm complexity increases with array size. Enormous computational burden
Bouselham [18], 2021	Fuzzy logic (FL)	Dynamic	1×1, 4×4	Employs a fuzzy logic-based controller to dynamically reconfigure the array	Experimentally analysed only for 1×1 PV array, highly infeasible for larger arrays
Rani [19], 2013	Sudoku	Static	9×9	Shade dispersion by sudoku puzzle pattern	Cannot be applicable other than 9×9 array sizes, there exists large no. of solutions available for sudoku puzzle and finding the optimal sudoku pattern is extremely challenging, first column is unchanged in some sudoku puzzles
Krishna [20], 2019	Optimal sudoku	Static	9×9	Shade dispersion by optimal sudoku pattern	
Rajani [21], 2021	Modified sudoku	Static	9×9	Shade dispersion by modified sudoku pattern	
Anjum [22], 2021	Hyper sudoku	Static	9×9	Shade dispersion by hyper sudoku pattern	
Rakesh [23], 2016	Magic square (MS)	Static	4×4	Physical relocation of panels using magic square pattern	Not applicable for all $n \times n$ arrays, not feasible for unsymmetrical PV arrays
Satpathy [24], 2017	Shade dispersion scheme	Static	3×3, 7×7	Shadow dispersion by optimal predefined interconnection of PV modules	Effectiveness compared only with conventional configurations and not tested for unsymmetrical arrays
Belhaouas [25], 2017	Shifted PV array arrangements	Static	9×9	Panels are arranged maximizing the distance between them within the array in different rows and columns	Underperforms under diagonal shading conditions
Nasiruddin [26], 2019	Odd-even pattern (OE)	Static	4×4	Reconfigured the panels using odd-even pattern	Despite being applicable to all arrays, optimal shade dispersal is not gained
Dhanalakshmi [27], 2018	Competence square	Static	9×9	Static technique following a unique renumbering pattern for panel relocation	Exhibits numerous MPPs imposing extra burden on MPPT controllers
Satpathy [28], 2018	Shade dispersion positioning	Static	3×3, 5×5	Distributes shade by repositing panels while electrical circuitry remains unaltered	After reconfiguration, $>$ 50% of the panels remain in same row of studied 3×3 array
Dhanalakshmi [29], 2018	Dominance square	Static	5×5	Reconfigures the conventional TCT array to mitigate row and column shading impact	Poor shade dispersion, very ineffective under diagonal shading conditions
Satpathy [30], 2019	Physical array relocation	Static	3×3, 5×5	One-time fixed configuration based on computational algorithm in MATLAB	Effectiveness of this scheme is yet to be verified for unsymmetrical arrays
Nihanth [31], 2019	Skyscraper puzzle	Static	9×9, 5×5	Yields more output compared to TCT, sudoku and DS techniques	Not applicable to all array sizes, and applicability to unsymmetrical array is challenging and not established
Satpathy [30], 2019	Fixed electrical reconfiguration	Static	4×3, 6×6	Employs electrical rewiring based on renumbering technique	Results compared only with conventional configurations
Desai [32] 2021	Hybrid conventional configurations	Static	6×6	Tested under 8 distinct shading cases, no of MPPs are reduced comparatively	Yields lower output compared to reconfigured PV arrays
Bonthagorla [33], 2020	Tripe-Tied configuration	Static	7×7	Number of interconnection ties requirement is reduced	Yields sub optimal solution to PS compared to reconfiguration schemes
Tatabhatla [34,35], 2019, 2020	Chaotic Baker's Map (CB)	Static	4×4, 6×6, 8×8	Reconfigures the panels using the concept of image encryption	Inadequate shade dispersal, incompatible for all symmetrical arrays and not feasible for $m \times n$ PV array sizes, generates many MPPs which burdens the MPPT controller
Reddy [36] 2020	Odd-even pattern (OE)	Static	9×9	Reconfigured the panels using odd-even pattern	Despite being applicable for $m \times n$ arrays, these techniques fail effective shade dispersion evenly over the entire array, yields numerous MPPs in the array's characteristics

(*continued*).

Table 1: Continued.

Author, year	Reconfiguration Technique	Type	Array size	Remarks	Limitations/shortcomings
Reddy [36] 2020	Odd-even-prime pattern (OEP)	Static	9×9	Reconfigured the panels using odd-even-prime pattern	
Venkateswari [37], 2020	Lo shu Square (LS)	Static	9×9	Physical relocation of panels using Lo Shu technique	Not applicable other than 9×9, not effective for all shading patterns
Madhanmohan [38], 2020	Diagonally dispersed TCT (DTCT)	Static	4×4	PV modules are rearranged diagonally in a TCT arrangement of PV array	50% of the panels in a row of an array remains unchanged
Chavan [39] 2021	Column & array reconfiguration	Static	5×5	PV module relocation performed within columns as well as within array	Relocation doesn't follow any particular method; it is executed randomly
Rakesh [40], 2022	Sequential Arrangement (SA)	Static	3×3, 9×9	PV panels of TCT configured array are dispersed column wise	Poor shade dispersion as many panels remains in same row after reconfiguration

being sophisticated, cannot obtain the entire potential of an array under shading. To enhance the array output above what is attainable by employing an MPPT controller solely, reconfiguration strategies of PV array are suggested [10]. The reconfiguration-techniques mitigate the multiple peaks in the array characteristics to a maximum extent and hence a simple MPPT algorithm such as Perturb and Observe is actually sufficient to track the GMP with maximum efficiency, low execution complexity, high accuracy, and higher tracking speed, eliminating the need for complex MPPT strategies. These array reconfiguration techniques are generally classified into static and dynamic techniques. Some of the notable reconfiguration techniques reported in the literature are given in Table 1.

Generally, the practical feasibility issues of dynamic reconfiguration techniques [11–18] are quite challenging due to their complex installation and operational issues. They necessitate systematic monitoring units, efficient driving circuits, complicated algorithms, complex controller units, a massive number of switches and sensors, increasing the system's complexity and cost. Due to the practical feasibility issues, cost-ineffectiveness of the dynamic reconfiguration techniques, the static ones are preferred. The static reconfiguration is a one-time reconfiguration and does not require switches, sensors, controllers and other additional equipment. Hence, it is a feasible and economical solution in mitigating the shading effects. However, from the literature review from Table 1, it is observed that a majority of the reported static reconfiguration techniques are applicable to only certain sizing of PV arrays and further cannot be generalized to other symmetrical and unsymmetrical array sizes. Furthermore, most of the techniques fail to rearrange the first column of the array and hence the shade in the first column remains unchanged thereby yielding sub optimal solution for shading-related problems. Also, a majority of these techniques fail to disperse the shade effectively and cannot be implemented for large-rated PV arrays. To rectify these issues, an efficient and generalized Henon map (HM) based reconfiguration technique is proposed in this paper to effectively disperse the shade by reconfiguring the modules. The proposed configuration is a practically feasible and viable solution as it is a fixed and one-time reconfiguration, which can be performed during the installation of the PV plant itself. Besides the associated technical feasibility, the proposed solution is also highly cost-effective as it does not require all the aforementioned devices and equipment for its operation. The installation and operational costs of the proposed configuration are very less compared to that of the existing dynamic reconfiguration strategies. The major highlights of the research work are:

- As contrasted with several static reconfiguration techniques, the proposed HM technique can be executed for both symmetrical and unsymmetrical sizes of PV array (*e.g.* $3 \times 3, 7 \times 11, 15 \times 17 \ldots$).
- To confirm the functionality and efficacy of the proposed HM configuration, the system is investigated with seven parameters for PV array of sizes 9×9, 8×8, 4×4, 3×5 and 4×3 during 19 shading conditions.
- The performance of the proposed technique is compared with the recently reported techniques such as Magic square [23], Odd-Even [26] – for 4×4, Chaotic Baker's Map [34,35], Odd-Even [36] – for 9×9, Odd-Even-Prime [36], Diagonal-TCT [38], and conventional SP and TCT [41] configurations. An inclusive technical analysis of row-current computations of various configurations during distinct shading cases has been presented.
- An experimental prototype of 4×4 PV array reconfiguration system is developed and tested under five shading conditions to demonstrate the superiority of the proposed technique.
- A quantitative and qualitative comparative assessment of the proposed technique with other state-of-art techniques is presented.

2. PV CELL MODELING

The output of PV cells is principally dependent on the incident solar irradiation and the temperature. Diverse mathematical models for modeling a PV cell are reported in the literature [42]. Due to its simplicity, a single-diode model is extensively employed. The output current (I) of PV cell is given as follows,

$$I = I_{Ph} - I_D - \frac{V_{PV} + IR_s}{R_{sh}} \quad (1)$$

$$I_D = I_0 \times \left[exp\left(\frac{V_D}{\alpha V_T}\right) - 1 \right] \quad (2)$$

$$I = I_{Ph} - I_0 \times \left[exp\left(\frac{V_D}{\alpha V_T}\right) - 1 \right] - \frac{V_{PV} + IR_s}{R_{sh}} \quad (3)$$

In Equation (3), "I_{ph}" denotes photocurrent, "I_0" denotes reverse saturation current, "V_D" denotes diode voltage, "V_T" denotes thermal voltage, "α" denotes ideality factor, "V_{PV}" denotes PV cell voltage "R_s," and "R_{sh}" denotes series and shunt resistances.

3. SETBACKS OF CONVENTIONAL ARRAY CONFIGURATIONS

Some of the distinguished conventional array configurations [41] reported in the literature are Series-Parallel (SP), Honey-Comb (HC), Bridge-linked (BL), and Total Cross Tied (TCT) configurations, as shown in Figure 1. Amongst these configurations, TCT configuration generates enhanced output under most of the shading condition. Nonetheless, all the conventional configurations hold a major drawback of zero-shadow distribution ability and thus resulting in increased mismatch losses under PS. To avoid these major disadvantages, the shade must be effectively dispersed by reconfiguring the array as discussed in the subsequent sections.

4. PROPOSED METHODOLOGY

In general, any digital image is considered to be composed of pixels in a 2D m × n matrix, where "m" and "n" denote the matrix rows and columns, respectively. In the image encryption process, the image is performed with a transformation by randomly replacing the original pixel locations of the image for security purposes [43]. Nonetheless, when the transformation is performed several times, the original image is retrieved. This is performed by altering the pixel locations of the image by employing a private-key algorithm that can be decoded by only end-users. In order to encrypt an image, popularly known 2D chaotic map algorithms are employed [44]. Generally, the two-dimensional maps are represented in the following form:

$$\begin{cases} x_{i+1} = r(x_i, y_i) \\ y_{i+1} = s(x_i, y_i) \end{cases} \quad (4)$$

where "r" and "s" are two given functions. By applying the chaotic map algorithm, the original pixel coordinates (x_i, y_i) of a digital image are repositioned to new pixel coordinates (x_{i+1}, y_{i+1}) to form an encrypted image for enhanced security purposes. The detailed process of scrambling of pixels for image encryption is shown in Figure 2. One of the well-known chaotic maps named HM is widely used in the encryption process is used.

4.1 Two-Dimensional Henon Chaotic Map

Henon Map is a two-dimensional invertible discrete-time non-linear dynamical system introduced by M. Henon in 1976 as a simplified demonstration for the Lorenz model. It is computationally effective and shows near-optimal randomness characteristic properties. The general mathematical equation of HM is described as follows [45]:

$$\begin{cases} x_{i+1} = (1 + y_i - ax_i^2) mod M, \\ y_{i+1} = (bx_i) mod M \end{cases} \quad (5)$$

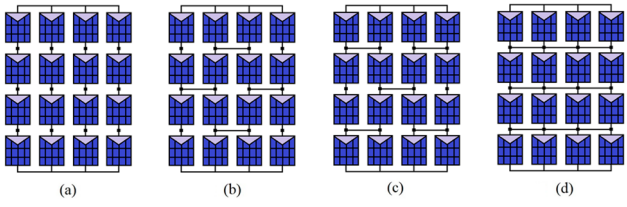

Figure 1: Conventional configurations: (a) SP, (b) HC, (c) BL and (d) TCT

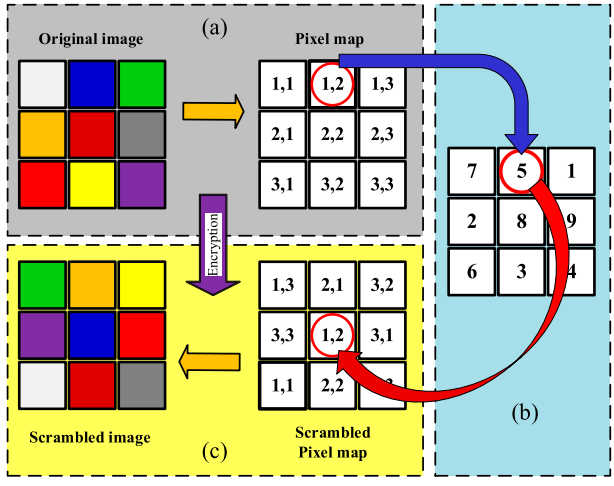

Figure 2: Image encryption process (a) Original image, (b) rearranged matrix and (c) scrambled image

The above map is a non-linear two-dimensional map, which is also similarly described as a dual-step recurrence relationship as follows:

$$x_{i+1} = 1 + bx_{i-1} - ax_i^2$$

where x' and "y" are continuous state variables, "i" is the number of iterations, "a" and "b" are control parameters and "M" denotes the order of the image that is to be encrypted. HM is generally examined in detail for $a = 1.4$ and $b = 0.3$, where the chaotic behavior is observed. The step-by-step formulation of the HM is described as follows [45]: To mimic the (a) stretching, (b) folding, and (c) reinjection that takes place in Lorenz chaotic system, Henon examined the subsequent series of mutations as presented in Figure 3. Firstly, a rectangle "Re" is extended along the horizontal x-axis as depicted in Figure 3(a). Later, the rectangle is stretched and folded by implementing the transformation described as follows:

$$T': \begin{cases} x' = x, \\ y' = 1 + y - ax^2, \end{cases} \tag{6}$$

where "a" is the degree of bending and the prime notation indicates the number of iterations. Here, the top and bottom regions of the rectangular "Re" gets mapped to parabolas as depicted in Figure 3(b). Subsequently, it is folded furthermore by compressing it along the horizontal x-axis:

$$T'': \begin{cases} x'' = bx', \\ y'' = y', \end{cases} \tag{7}$$

where $|b| < 1$. The region is compressed for $|b| < 1$. This, in turn, yields Figure 3(c). Eventually, the region is oriented along x-axis by reflecting over the "$y = x$" line as shown in Figure 3(d). This is called re-injection.

$$T''': \begin{cases} x''' = y'', \\ y''' = x'', \end{cases} \tag{8}$$

Then the combined transformation, $T_r = T_r'''(T_r''(Tr'(Re)))$ will give the chaotic Henon mapping given in Equation (5) as shown below, where (x_i, y_i) is the initial state of (x, y) and $(x_{i+1}; y_{i+1})$ is the next state of $(x'''; y''')$.

$$\begin{matrix} x''' = y'' \\ y''' = x'' \end{matrix} \Rightarrow \begin{matrix} x''' = y' \\ y''' = bx' \end{matrix} \Rightarrow \begin{cases} x''' = 1 + y - ax^2, \\ y''' = bx, \end{cases}$$

$$\Rightarrow \begin{cases} x_{i+1} = 1 + y_i - ax_i^2, \\ y_{i+1} = bx_i \end{cases} \tag{9}$$

A standard Henon chaotic map has discrete-time, nevertheless, the state variables "x" and "y" are continuous in nature. So, in order to expedite the discrete digital image processing, a discrete HM [46] is defined by the following equation

$$\begin{cases} x_{i+1} = (1 - ax_i^2 + y_i) \mod M \\ y_{i+1} = (x_i + c) \mod M \end{cases} \tag{10}$$

where x and y are the state variables discrete in nature belonging to (0, 1, 2, 3, …… ., M-1). In Equation (10), "a" and "c" are two controlling parameters. The 2D HM is an invertible map and the inverse transformation of it is described as follows:

$$\begin{cases} x_i = \dfrac{y_{i+1}}{b}, \\ y_i = x_{i+1} - 1 + \dfrac{ay_{i+1}^2}{b^2} \end{cases} \tag{11}$$

By applying the mathematical equation of the HM algorithm, all the original pixel coordinates of a 4×4 matrix are repositioned to new pixel coordinates as detailed in the flowchart shown in Figure 4. The original matrix elements and the rearranged matrix obtained by the proposed HM for an 8×8 array is shown in Figure 5(a) and 5(d).

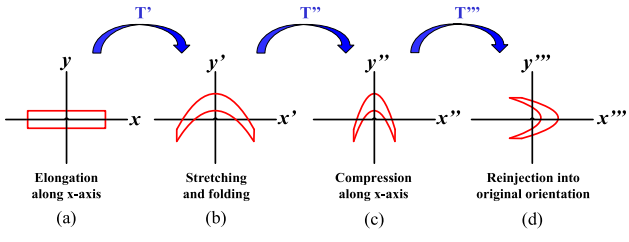

Figure 3: Sequence of transformations "T" for one iteration of Henon Map

4.2 Application of HM in Array Reconfiguration

The principal objective of image encryption is to minimize the correlation between adjacent pixels in a digital image. As the digital image comprises numerous pixels, the PV array is also composed of many solar panels connected in series and parallel to obtain the rated output as shown in Figure 6. The image encryption concept is applied here by considering an individual PV panel as a pixel of an image, and the whole PV array as an image consisting of pixels. As the pixels of an image are rearranged by encryption, the panels in the array are reconfigured based on the rearranged matrix pattern obtained by HM in order to disperse the shade evenly over the array. The shade is dispersed by replacing the modules in such a way that the correlation between two adjacent shadowed modules in a row is mitigated thereby attaining equal irradiation among rows with reduced mismatches. For instance, it is noted from Figure 6 that the panel

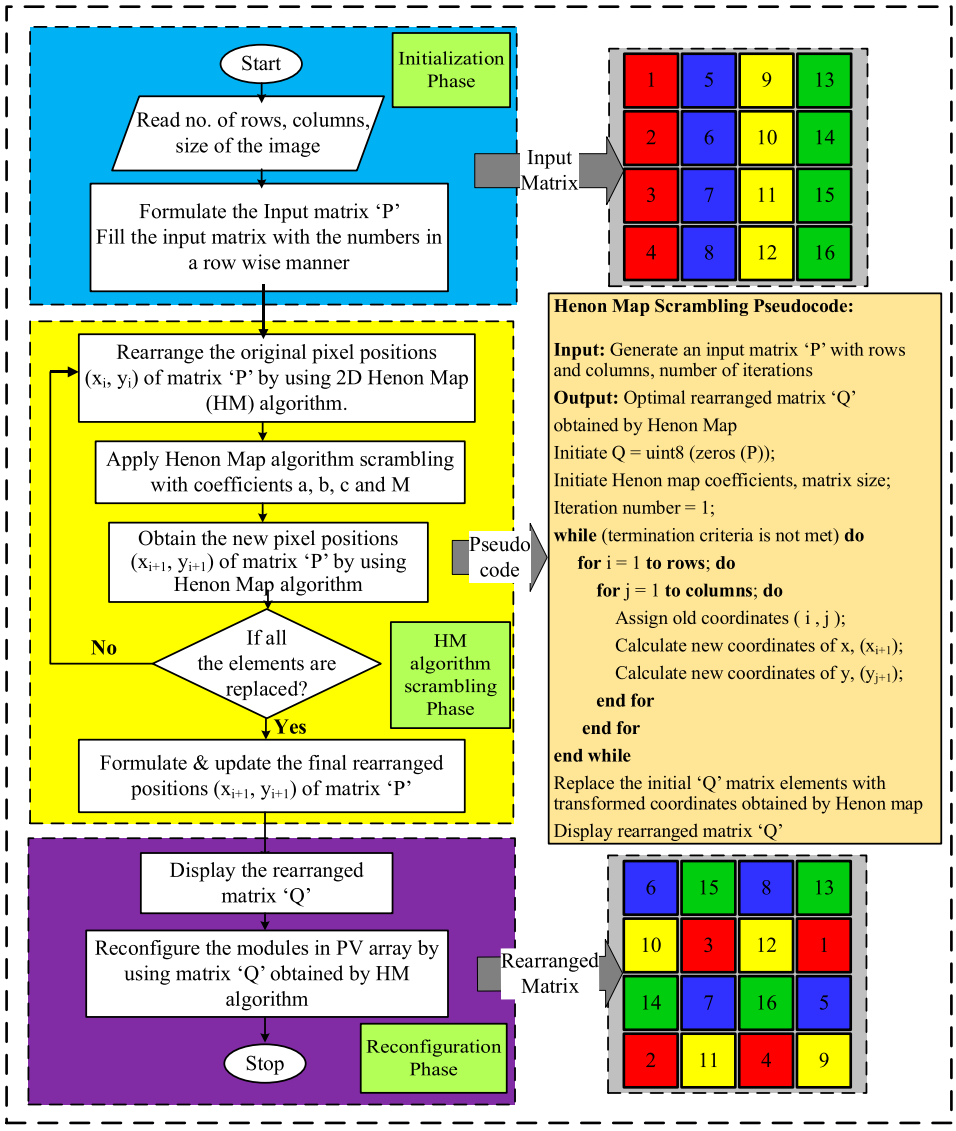

Figure 4: Flowchart of HM-based PV array reconfigurtaion

1	9	17	25	33	41	49	57
2	10	18	26	34	42	50	58
3	11	19	27	35	43	51	59
4	12	20	28	36	44	52	60
5	13	21	29	37	45	53	61
6	14	22	30	38	46	54	62
7	15	23	31	39	47	55	63
8	16	24	32	40	48	56	64

(a)

14	63	16	57	10	59	12	61
22	7	24	1	18	3	20	5
30	15	32	9	26	11	28	13
38	23	40	17	34	19	36	21
46	31	48	25	42	27	44	29
54	39	56	33	50	35	52	37
62	47	64	41	58	43	60	45
6	55	8	49	2	51	4	53

(b)

Figure 5: (a) Original 8 × 8 matrix and (b) its corresponding reaaranged matrix obtained by proposed HM technique

"29" of 9 × 9 PV array located in (2,4) coordinates and when applied with HM, it is now moved to (3,5) coordinates. Similarly, the panel "34" that is originally located in (7,4) coordinates is now moved to (5,1) coordinates. Likewise, all the panels of the 9 × 9 array are effectively rearranged employing HM technique attaining least mismatch between the panels of an array under shading conditions.

4.3 Evolution of HM Based PV Array Reconfiguration

To improve the array output under shading, PV panels are optimally interconnected in a predefined configuration. The novel HM approach is the highly suitable solution that can be employed in the optimal array reconfiguration of TCT as it disperses the shade uniformly in all the rows without disturbing the electrical circuitry. This does not induce any difference in its electrical properties while diminishing the shading impact. The PV panels in TCT are physically relocated based on rearranged HM matrix

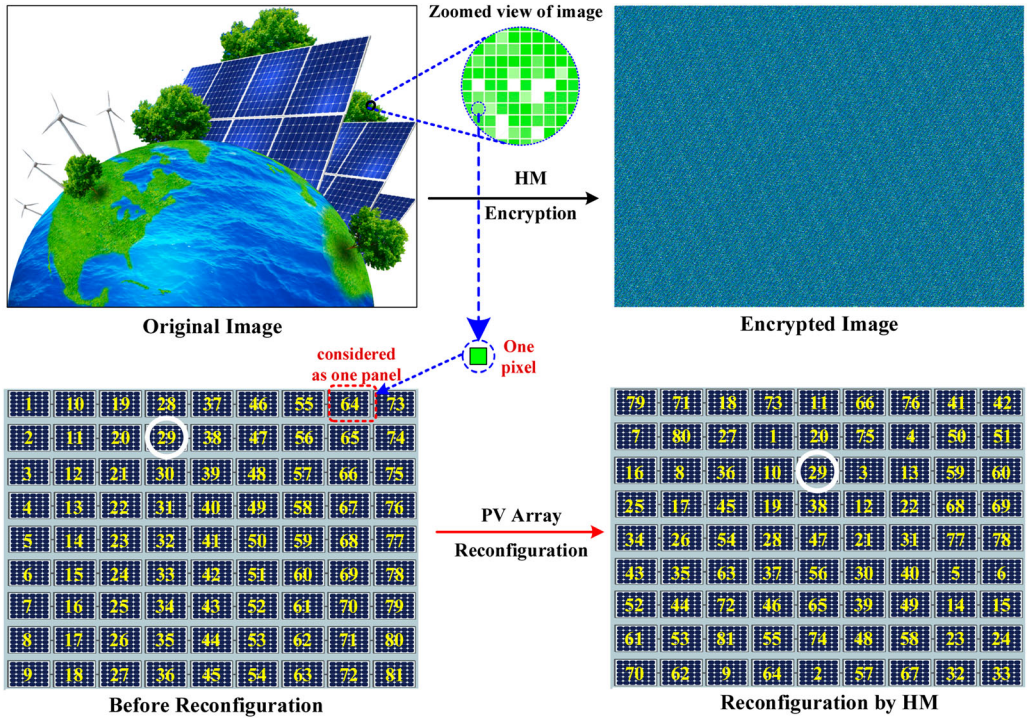

Figure 6: Pictorial representation of applicability of HM encryption algorithm in array reconfiguration

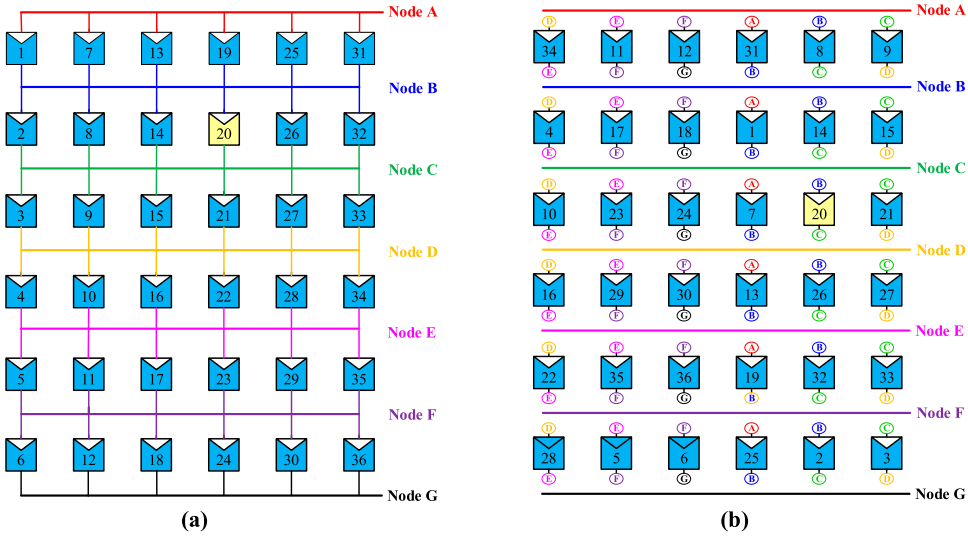

Figure 7: Structural arrangement of PV panels in (a) TCT and (b) HM configurations of 6 × 6 array without altering electrical circuitry

and the structural difference in the arrangement between conventional TCT and the proposed HM arrangement with new locations of the panels in an array is shown in Figure 7.

All the panels are denoted with the nodes on either side of the PV panels, which symbolizes that they are electrically interconnected to the same row. From Figure 7(a), it is noted that the panel number "20" is in the second row and the fourth column of the conventional TCT configuration connected between Node-B and Node-C, and this panel is physically relocated to the third row and the fifth column, *i.e.* in between Node-C and Node-D (based on the HM rearranged matrix) as shown in Figure 7(b). Similarly, all the panels are optimally reconfigured based on the rearranged HM matrix to disperse the shade evenly. Suppose if the first row of the HM-configured array with panel numbers 34, 11, 12, 31, 8, and 9 are shaded, the shade is equally distributed over the entire array equalizing the irradiation in rows as these panels are physically located in the first row but electrically connected to distinct rows of an array. In consequence, the proposed

image encryption-based panel reconfiguration strategy maximizes the energy harvest.

5. RESULTS AND DISCUSSION

The considered PV array configurations of various sizes such as 9 × 9, 8 × 8, 4 × 4, 3 × 5, and 4 × 3 are executed in a MATLAB simulation environment and tested under distinct uniform and non-uniform shading conditions. A variable-step type, ode23tb (stiff/TR-BDF2) solver is used in the computation of the states of the model during the simulation. The maximum and minimum step size of the solver is set to the default value (auto) and the relative tolerance is set to 1e-4. A KG200GT-200W panel is considered for simulation studies, and its specifications are given in Table A1 of Appendix. The following parameters [37] are considered for the evaluation of configurations:

- Mismatch Power Loss, $\mathrm{MPP_L}(\%) = \frac{\mathrm{GMP_{STC}} - \mathrm{GMP_{PS}}}{\mathrm{GMP_{STC}}}$
- Fill Factor, $\mathrm{FF} = \frac{\mathrm{V_{MPP}} * \mathrm{I_{MPP}}}{\mathrm{V_{oc}} * \mathrm{I_{sc}}}$
- Efficiency, $\eta(\%) = \frac{\mathrm{V_{MPP}} * \mathrm{I_{MPP}}}{G \times A}$
- Array Yield, $Y_\mathrm{A}(\mathrm{h/day}) = \mathrm{kWh/kW_p/day}$
- Performance Ratio, $\mathrm{PR}(\%) = \frac{Y_\mathrm{Final}}{Y_\mathrm{ref}}$
- No. of Maximum Power Peaks (MPPs)

where $\mathrm{GMP_{STC}}$ is GMP at standard test conditions, $\mathrm{GMP_{PS}}$ is GMP at PS, $\mathrm{V_{MPP}}$ and $\mathrm{I_{MPP}}$ is the voltage and current at maximum power, $\mathrm{V_{OC}}$ and $\mathrm{I_{SC}}$ is the open-circuit voltage and short circuit current, "G" is solar irradiation ($\mathrm{W/m^2}$) and A is the area of panel, kWh is actual energy yield, $\mathrm{kW_p}$ is the rated array output, Y_Final and Y_ref are the final and reference array yield (Tables 2 and 3).

5.1 Analysis of 9 × 9 PV Array

To validate the effectiveness of the proposed technique, four distinct shading patterns from Case 1–4 are considered for analysis. The obtained results are compared with the very recently reported Odd-Even, OE [36], and Odd-Even-Prime, OEP [36], array configurations. Table 4 gives the comparison of performance parameters of 9 × 9 array under various shading conditions. The analysis is as follows.

Table 2: Row current variation of various configurations of 9 × 9 array

	Row current	TCT [41]	OE [36]	OEP [36]	HM
Case-1	Min	4.6 I_m	5.6 I_m	6.6 I_m	7.6 I_m
	Max	8.1 I_m	8.1 I_m	8.1 I_m	8.1 I_m
Case-2	Min	4.6 I_m	5.6 I_m	5.6 I_m	6.1 I_m
	Max	8.1 I_m	8.1 I_m	7.1 I_m	8.1 I_m
Case-3	Min	0.9 I_m	4.9 I_m	3.3 I_m	6.3 I_m
	Max	8.1 I_m	8.1 I_m	7.3 I_m	6.3 I_m
Case-4	Min	4.9 I_m	4.9 I_m	5.7 I_m	6.1 I_m
	Max	8.1 I_m	8.1 I_m	8.1 I_m	8.1 I_m

Table 3: Row current variation of various configurations of 8 × 8 array

	Row current	TCT [41]	CB [35]	HM
Case-1	Min	4.2 I_m	6.2 I_m	6.7 I_m
	Max	7.2 I_m	7.2 I_m	7.2 I_m
Case-2	Min	4.2 I_m	5.2 I_m	5.7 I_m
	Max	7.2 I_m	6.7 I_m	7.2 I_m
Case-3	Min	0.8 I_m	4.0 I_m	5.4 I_m
	Max	7.2 I_m	7.2 I_m	5.4 I_m
Case-4	Min	4.8 I_m	5.2 I_m	5.4 I_m
	Max	7.2 I_m	7.2 I_m	7.2 I_m

Table 4: Comparison of performance parameters of 9 × 9 array

Config.	GMP (W)	$\mathrm{MMP_L}$ (%)	FF	η (%)	$\mathrm{Y_{A(hr/day)}}$	PR (%)	MPPs
Case-1							
SP [41]	13,152	10.274	0.680	13.433	5.383	89.725	2
TCT [41]	12,986	11.406	0.671	13.263	5.315	88.593	2
OE [36]	12,348	15.759	0.638	12.612	5.054	84.240	3
OEP [36]	13,112	10.547	0.678	13.392	5.367	89.452	3
HM	13,905	5.137	0.719	14.202	5.691	94.86	2
Case-2							
SP [41]	8761.3	40.228	0.453	10.543	3.586	59.771	2
TCT [41]	9145	37.610	0.473	11.005	3.743	62.389	2
OE [36]	10,900	25.637	0.564	13.117	4.461	74.362	5
OEP [36]	11,141	24.00	0.576	13.407	4.560	76.006	4
HM	11,355	22.533	0.587	13.665	4.647	77.466	2
Case-3							
SP [41]	9641.7	34.222	0.498	12.053	3.946	65.777	4
TCT [41]	9641.7	34.222	0.498	12.053	3.946	65.777	4
OE [36]	9969.6	31.985	0.515	12.463	4.080	68.014	6
OEP [36]	9734.9	33.586	0.558	12.170	3.984	66.413	6
HM	11,404	22.199	0.758	14.256	4.668	77.801	1
Case-4							
SP [41]	10,642	27.398	0.550	11.623	4.356	72.601	2
TCT [41]	10,325	29.560	0.534	11.277	4.226	70.439	2
OE [36]	11,166	23.823	0.577	12.195	4.570	76.176	4
OEP [36]	11,572	21.053	0.598	12.639	4.736	78.946	4
HM	11,821	19.354	0.611	12.910	4.838	80.645	2

5.1.1 During Case-1 Shading Condition

In this case, seven panels of the first row in a PV array are shaded thereby receiving 0.4 $\mathrm{kW/m^2}$ and the unshaded modules receive 0.9 $\mathrm{kW/\ m^2}$, as shown in Figure 8(a).

The respective row current variation of TCT, OE, OEP, and HM is 4.6Im to 8.1Im, 5.6Im to 8.1Im, 6.6Im to 8.1Im, and 7.6Im to 8.1Im (Table 2). The HM technique effectively disperses the shade yielding the least current variation and mismatches. In this case, the SP, TCT, OE, OEP, and HM configurations yield the GMP of 13152W, 12986W, 12348W, 13112W, and 13905W. It is noted that the existing OE yields 6.19% and 4.92% less power than SP and TCT, whereas the OEP technique yields only

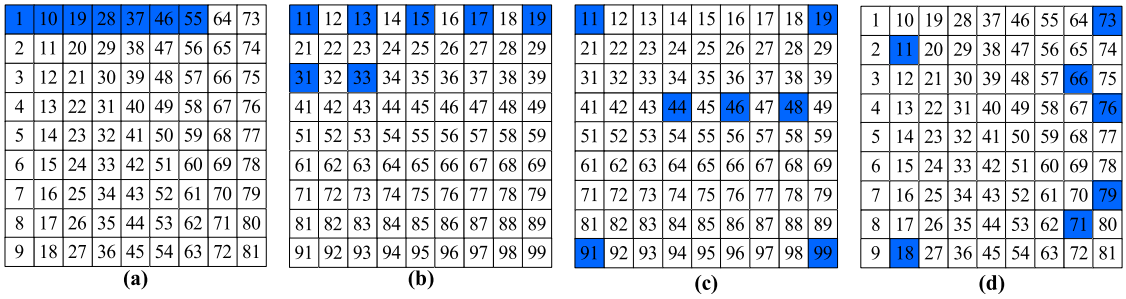

Figure 8: Case-1: (a) shading in TCT, shade dispersal by (b) OE [36], (c) OEP [36], and (d) HM

0.97% more GMP than TCT. However, the HM configuration yields 753W, 919W, 1557W, and 793W more power compared to SP, TCT, OE, and OEP, respectively. The proposed HM technique gives 7.08% enhancement in GMP. Additionally, the MPPs obtained by HM are also comparatively reduced. From Figure 17(a), it is noted that the HM gives smoother characteristics compared to all other configurations.

5.1.2 During Case-2 Shading Condition

During this condition, twenty-eight panels of the first four rows of the PV array are shaded as shown in Figure 9(a).

Both SP and TCT configurations yield the most inferior performance with broad variation in row currents ranging from 4.6Im to 8.1Im, whereas OE, OEP, and HM configuration offer 5.6Im to 8.1Im, 5.6Im to 7.1Im and 6.1Im to 8.1Im, respectively. The respective OE and OEP techniques exhibit five and four power peaks in the characteristics as shown in Figure 17(b), whereas the HM technique exhibit only two peaks resulting smoother characteristics with the highest GMP. The HM configuration yields 2593.7, 2210, 455, and 214 W more power compared to SP, TCT, OE, and OEP, which is 22.85%, 19.47%, 4.01%, and 1.89%, respectively.

5.1.3 During Case-3 Shading Condition

In this case, the center part of the array is considered to be non-uniformly shaded by a commonly occurring short broad typed shading pattern, as shown in Figure 10(a).

The shaded and unshaded modules receive irradiation of (0.1-0.5) kW/m^2 and 0.9 kW/m^2, respectively. The conventional SP and TCT configurations yield the lowest GMP with a very broad range of row currents varying

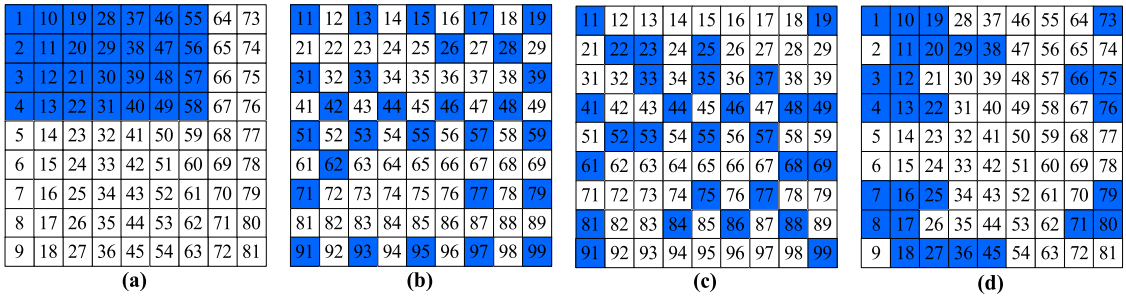

Figure 9: Case-2: (a) shading in TCT, shade dispersal by (b) OE [36], (c) OEP [36], and (d) HM

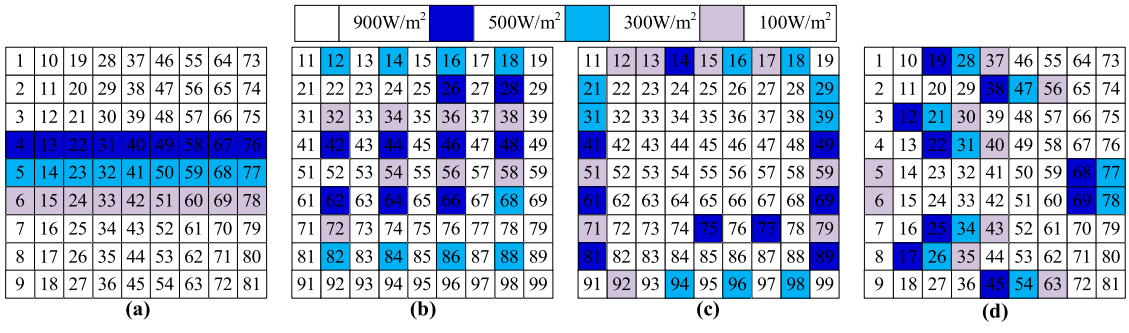

Figure 10: Case-3: (a) shading in TCT, shade dispersal by (b) OE [36], (c) OEP [36], and (d) HM

from 0.9Im to 8.1Im. The existing OE and OEP also exhibit broad variation from 4.9Im to 8.1Im and 3.3Im to 7.3Im, respectively. On the contrary, HM exhibits zero row current variation with only one power peak, whereas SP, TCT, OE, and OEP exhibits four, four, six, and six power peaks in the characteristics as shown in Figure 17(c). The proposed HM configuration yield 1762.3, 1762.3, 1434.4, and 1669.1W more GMP, which is 18.28%, 18.28%, 14.39%, and 17.15% higher compared to SP, TCT, OE, and OEP, respectively. HM yields superior performance with the highest GMP (11,404 W), lowest mismatch (22.199 W), highest FF (0.758), highest efficiency (14.256%), highest array yield (4.668), and highest PR (77.801%).

5.1.4 During Case-4 Shading Condition:

Under Case-4, a corner part of an array is non-uniformly shaded by a short narrow shading pattern, as shown in Figure 11(a).

During this case, the respective row current variation of TCT, OE, OEP, and HM configurations is 4.9Im to 8.1Im, 4.9Im to 8.1Im, 5.7Im to 8.1Im, and 6.1Im to 8.1Im. A comparatively narrow row current variation is obtained with HM configuration. Further, from Figure 17(d), it is noted that both OE and OEP configurations exhibit four MPPs, respectively, whereas HM configuration exhibits only two MPPs. The respective GMP obtained by SP, TCT, OE, OEP, and HM configurations is 10,642; 10,325; 11,166; 11,572; and 11,821 W. The HM configuration gives 1179, 1496, 655, and 249 W more power than SP, TCT, OE, and OEP, respectively. It is evident in all the shading cases considered for 9×9 array, the proposed HM configuration yields superior performance with enhanced values of GMP, MMP_L, F.F, η, P.R, Y_A as given in Table 4. The minimum and maximum row currents of various configurations of 9×9 array are given in Table 2.

5.2 Analysis of 8 × 8 PV Array

To demonstrate the compatibility of the proposed technique to 8×8 arrays, the same type of shading patterns considered for 9×9 arrays is considered for analysis. The obtained results are compared with the recently reported Chaotic Baker's Map, CB [35] reconfiguration technique for an 8×8 array. The comparison of performance parameters of 8×8 array under various shading conditions is given in Table 5. The row current variation of TCT, CB, and HM configurations of an 8×8 PV array is given in Table 3. The analysis is as follows:

5.2.1 During Case-5 Shading Condition

During this case, six modules of the first row in a PV array are shaded, thereby receiving 0.4 kW/m^2 and the unshaded modules receive 0.9 kW/m^2, as shown in Figure 12(a). Due to its inability to disperse the shade, the TCT configuration yields a wide variation in row

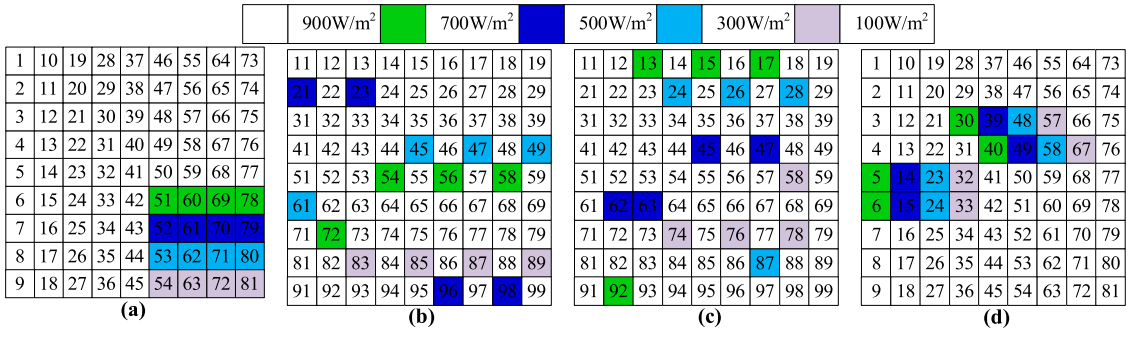

Figure 11: Case-4: (a) shading in TCT, shade dispersal by (b) OE [23], (c) OEP [23], and (d) HM

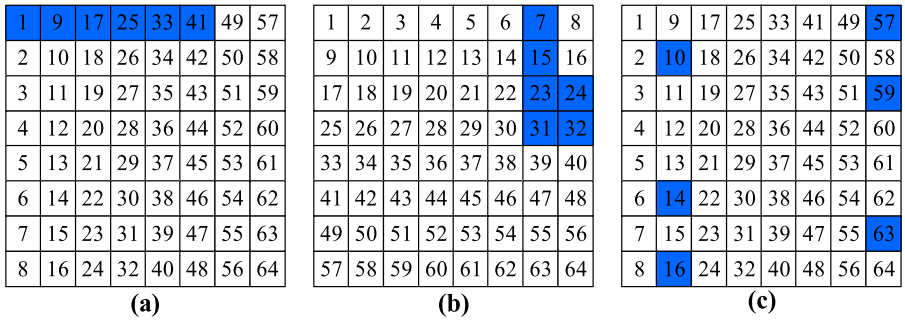

Figure 12: Case-5: (a) shading in TCT, shade dispersal by (b) CB and (c) HM

Table 5: Comparison of performance parameters of 8 × 8 array

Config.	GMP (W)	MMP_L (%)	FF	η (%)	$Y_{A(hr/day)}$	PR (%)	MPPs
Case-5							
SP [41]	10,249	11.50	0.665	13.305	5.309	88.49	2
TCT [41]	10,095	12.83	0.655	13.105	5.229	87.16	2
CB [35]	10,616	8.34	0.689	13.782	5.499	91.65	3
HM	10,918	5.73	0.709	14.175	5.657	94.27	2
Case-6							
SP [41]	7255.6	37.35	0.471	10.582	3.758	62.64	2
TCT [41]	7500.5	35.24	0.486	10.939	3.885	64.75	2
CB [35]	9088.8	21.52	0.634	13.256	4.708	78.47	3
HM	9424.3	18.62	0.612	13.746	4.883	81.38	2
Case-7							
SP [41]	7122.7	38.50	0.462	11.687	3.689	61.49	4
TCT [41]	7122.7	38.50	0.462	11.687	3.689	61.49	4
CB [35]	7137.4	38.37	0.463	11.711	3.697	61.62	4
HM	8688.8	24.98	0.753	14.257	4.502	75.02	1
Case-8							
SP [41]	8748.7	24.46	0.568	11.880	4.532	75.53	4
TCT [41]	8750.5	24.44	0.568	11.882	4.533	75.55	4
CB [35]	9368.6	19.10	0.607	12.722	4.853	80.89	5
HM	9461.7	18.30	0.615	12.849	4.902	81.70	2

currents ranging from 4.2Im to 7.2Im. The existing CB configuration yields the variation from 6.2Im to 7.2Im. By employing the proposed HM configuration, a narrow row current variation is obtained in the range of 6.7Im to 7.2Im, thereby reducing the multiple peaks in the PV characteristics as shown in Figure 17(e).

The CB and HM configuration exhibits three and two MPPs. The GMP obtained by TCT, CB, and HM configurations is 10,095 W; 10,616 W; and 10,918 W. The P_L obtained in TCT and CB configurations is 12.83% and 8.34%, whereas the HM configuration yields lesser MPP_L of 5.73%.

5.2.2 During Case-6 Shading Condition

During this condition, eighteen modules of the first three rows of PV array are shaded as shown in Figure 13(a). The row current variation of TCT, CB, and HM configurations is 4.2Im to 7.2Im, 5.2Im to 6.7Im, and 5.7Im to 7.2Im (Table 3).

The narrow row current variation is obtained by HM configuration, thereby rendering smoother PV characteristics with reduced MPPs, as shown in Figure 17(f). HM configuration enhances GMP by 25.65% and CB enhances by only 21.17%. When compared to CB, the GMP of 335.5 W more is obtained by HM configuration. Further, HM configuration gives the lowest MMP_L of 2157.7 W compared to TCT (4081.5 W) and CB (2493.2 W). With HM configuration, the power loss is almost reduced by half, which is from 35.24% to 18.6%.

5.2.3 During Case-7 Shading Condition

In this case, a commonly occurring short broad typed non-uniform shading pattern as shown in Figure 14(a) is considered.

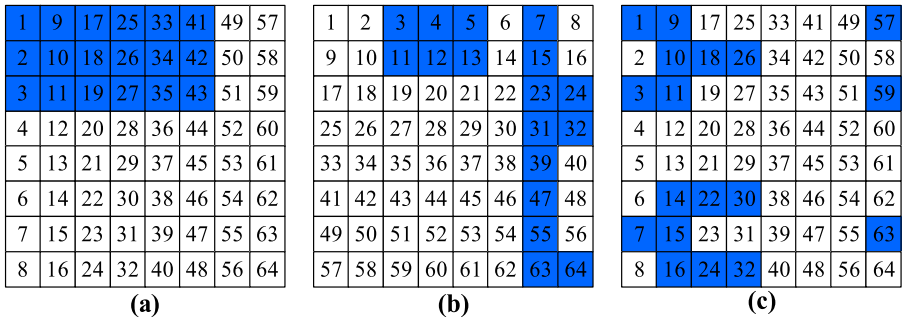

Figure 13: Case-6: (a) shading in TCT, shade dispersal by (b) CB and (c) HM

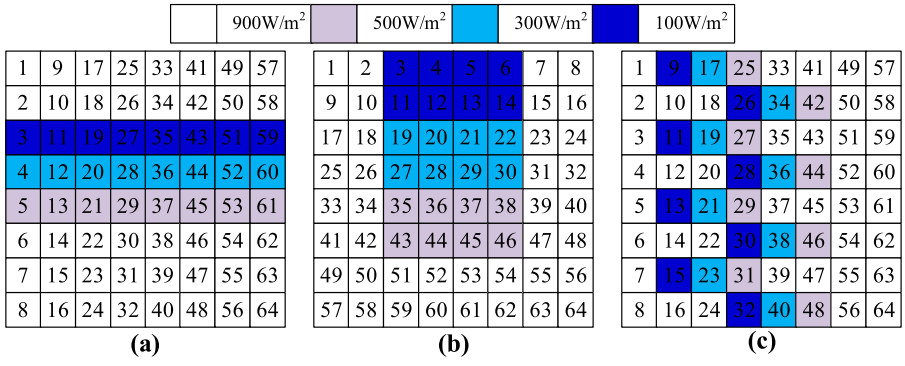

Figure 14: Case-7: (a) shading in TCT, shade dispersal by (b) CB and (c) HM

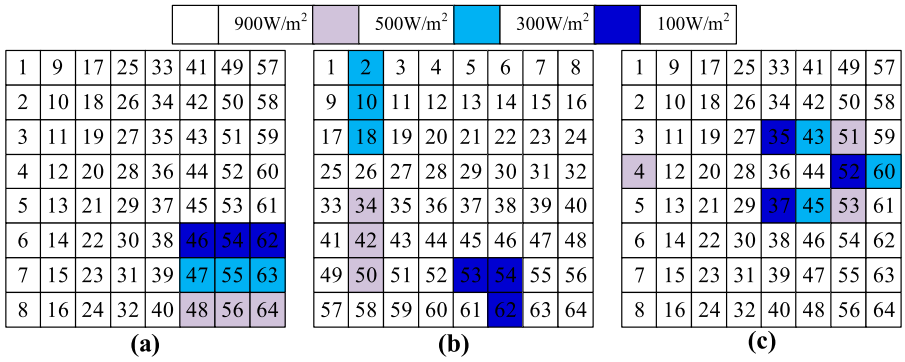

Figure 15: Case-8: (a) shading in TCT, shade dispersal by (b) CB and (c) HM

The TCT configuration gives poor performance offering a very broad range of row currents varying from 0.8Im to 7.2Im, whereas CB offers 4.0Im to 7.2Im. This wide variation is further reduced by the proposed HM configuration in which all rows generate 5.4Im, thereby yielding only one MPP with smoother PV characteristics, as shown in Figure 17(g). On the contrary, both TCT and CB configurations yield four MPPs. The GMP obtained by TCT, CB, and HM configurations is 7122.7, 7137.4 and 8688.8 W, respectively. When compared to TCT and CB, the output is enhanced by 1566.1 and 1551.4 W, which is 21.99% and 21.79%, respectively. The MM_L is significantly reduced from 4459.3 W to 2893.2 W with the proposed HM technique.

5.2.4 During Case-8 Shading Condition

During Case-8, corner part of an 8×8 array is non-uniformly shaded by a short narrow pattern, as shown in Figure 15(a).

The respective row current variation of TCT, CB, and HM configurations under this case is 4.8Im to 7.2Im, 5.2Im to 6.7Im, and 5.4Im to 7.2Im. The GMP obtained by TCT, CB, and HM configurations is 8750.5, 9369.1, and 9396.6 W, respectively. The respective GMP enhancement by CB and HM configurations is 7.06% and 7.39% with respect to TCT. Despite its effectiveness in augmenting GMP compared to TCT, CB configuration generates five MPPs which are closely observed in characteristics. By employing HM configuration, highest output is obtained along with only two MPPs resulting in smoother PV characteristics, as shown in Figure 17(h).

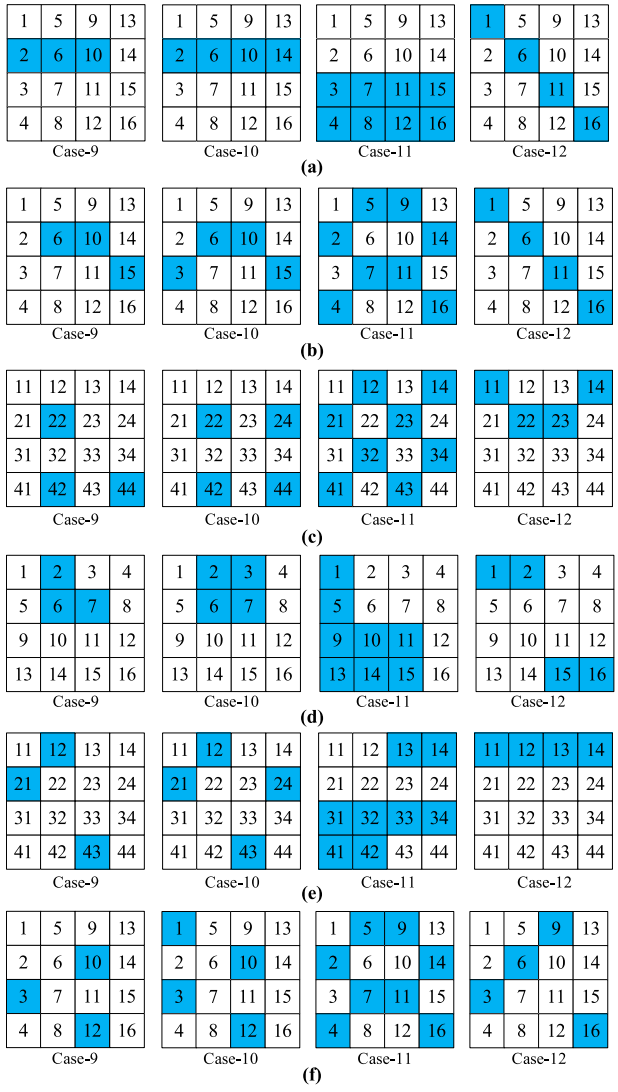

Figure 16: Case-9 to Case-12 shading in (a) TCT, shade dispersal by (b) MS [23], (c) OE [26], (d) CB [34], (e) DTCT [38], and (f) HM

5.3 Analysis of 4 × 4 PV Array

To demonstrate the compatibility and effectiveness of the proposed technique for small rated PV arrays, a 4×4 PV array is tested under four distinct uniform shading patterns as shown in Figure 16(a). The modules receive 0.4 and 0.9 kW/m^2 during shading and non-shading conditions, respectively. The obtained results are compared with TCT [41] and other notable reconfiguration techniques such as Magic square, MS [23], Odd-Even, OE

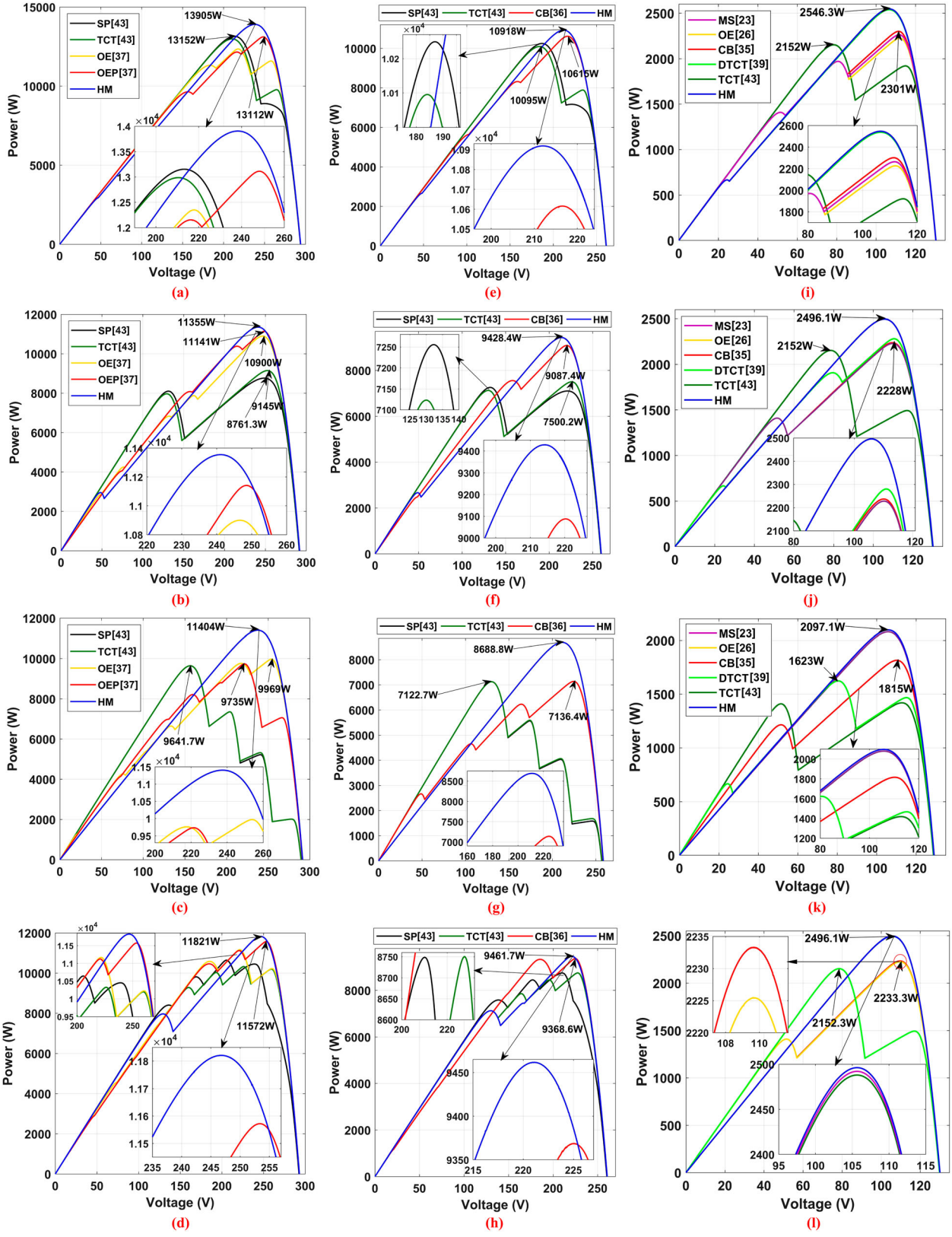

Figure 17: Power-Voltage (PV) charcteristics of various configurations under (a–d) Case-1 to Case-4 of 9 × 9 array, (e–h) Case-5 to Case-8 of 8 × 8 array, and (i–l) Case-9 to Case-12 of 4 × 4 PV arrays, respectively

Table 6: Comparison of GMP and MPPs of various configurations of 4 × 4 array

	GMP in Watt (number of MPPs)			
Config.	Case-9	Case-10	Case-11	Case-12
TCT [41]	2152.3 (2)	2152.0 (2)	1418.9 (2)	2494.9 (1)
MS [23]	2263.3 (3)	2228.2 (2)	2096.4 (1)	2496.0 (1)
OE [26]	2225.4 (3)	2227.1 (2)	2096.5 (1)	2233.3 (2)
CB [34]	2301.0 (3)	2237.1 (2)	1815.2 (2)	2233.3 (2)
DTCT [38]	2546.0 (2)	2280.6 (2)	1623.0 (3)	2152.3 (2)
HM	2546.3 (2)	2496.1 (1)	2097.1 (1)	2496.1 (1)
Best config.	HM, DTCT	HM	HM, MS, OE	HM, MS

[26], Chaotic Baker's Map, CB [34], and Diagonal-TCT, DTCT [38].

The corresponding PV characteristics of various configurations for a 4 × 4 PV array are shown in Figure 17(i)–(l). From the results, the following analysis is made: During Case-9, the HM configurtaion yielded 18.306%, 12.51%, 14.42%, 10.67%, 0.02% more GMP when compared to TCT, MS, OE, CB, and DTCT.

During Case-10, the proposed HM outperformed all techniques by enhancing the GMP by 15.99%, 12.03%, 12.082%, 11.58%, and 9.45% compared to TCT, MS, OE, CB, and DTCT configurtaions. Further under Case-11, the HM yields 47.79%, 15.53%, and 29.22% more GMP compared to TCT, CB, and DTCT configurtaions, whereas the performance of MS and OE is on par with HM. During Case-12, HM yielded 11.77%, 11.76%, and 15.98% more GMP when compared to OE, CB, and DTCT. In Case-11 and Case-12, the performance of MS is on par with HM, however, in Case-9 and Case-10, MS yields 12.5% lower output and more MPPs compared to HM. Moreover, the major limitation of MS technique is that it can be employed only for very few square matrices and not for others. It is evident from the array characteristics in Figure 17(i)–(l) that the proposed HM yields the highest GMP, less MPPs, superior shade dispersion, and lowest mismatch when compared to all other techniques. Table 6 gives the comparative analysis of GMP and MPPs obtained for a 4 × 4 PV array under Case-9 to Case-12.

5.4 Experimental Validation of Proposed Reconfiguration Technique for 4 × 4 PV Array

To validate the supremacy of the proposed HM configuration over existing MS [23], OE [26], and CB [34] configurations, a 4 × 4 PV array reconfiguration system is developed and experimented as shown in Figure 18. A 16 number of 3W panels are connected in MS, OE, and CB and HM configurations are considered for analysis. The panel specifications are given in Table A1 of the appendix. The PV array is connected to a variable rheostat, and

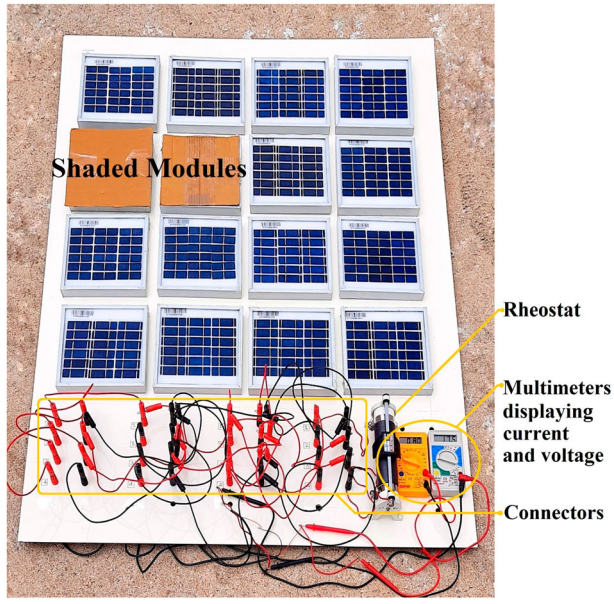

Figure 18: Experimental protoype of 4 × 4 array reconfiguration system

two digital multimeters are employed to measure the array voltage and current. The PV modules are connected in various MS, OE, CB, and proposed HM configurations with the help of banana connectors, as shown in the experimental setup. The experiment is carried out in an outdoor environment during noontime. The artificial shading blocks are used to shade the modules to create desired shading patterns of Case-13 to Case-17, as shown in Figure 19. Shading cases from 13 to 14 resemble the progressive movement of a passing cloud over array; further triangular, diagonal, and zig-zag patterns are considered in Case-15 to Case-17, respectively.

The respective PV characteristics under case-13 to 17 are shown in Figure 21(a)–(e). It is evident from Figure 20 that the proposed HM configuration yields enhanced output compared to existing MS, OE, and CB in all cases due to its better shade dispersion capability, as seen in Figure 19(e). From the analysis it is noted that the obtained experimental results shown in Figure 20 are close to the simulation results (Figure 21). The proposed HM eliminates the drawbacks of existing techniques by evenly dispersing the shade, reducing the row current variation, thereby enhancing the GMP significantly.

5.5 Compatibility and Extension of HM Technique to Unsymmetrical m × n Arrays:

A majority of the static reconfiguration techniques proposed in the literature, including MS [23] and CB [34,35] are not compatible with all n × n PV arrays. Further, the

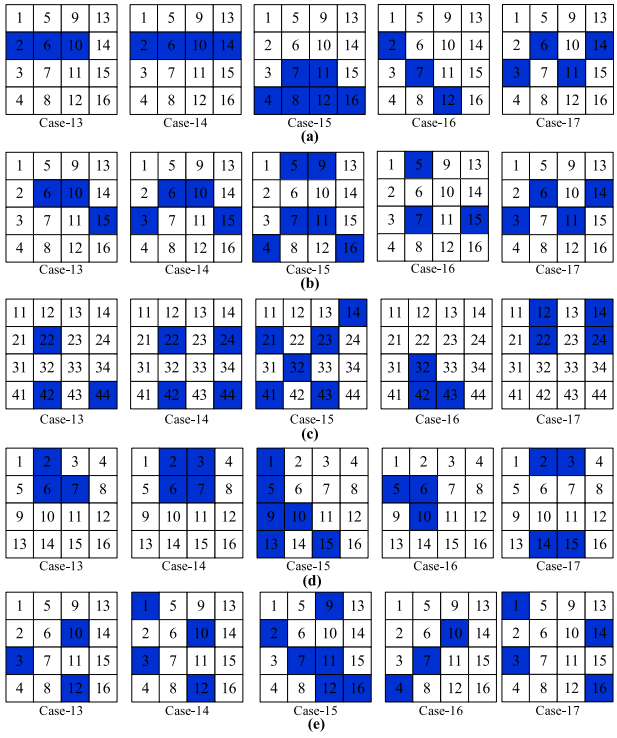

Figure 19: Case-13 to Case-17 shading in (a) TCT, shade dispersal by (b) MS [23], (c) OE [26], (d) CB [34], and (e) HM configurations

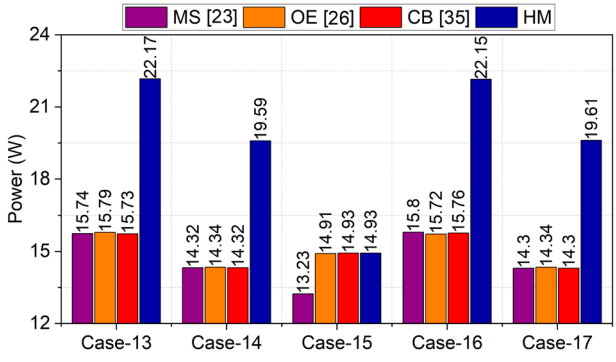

Figure 20: Output of a 4 × 4 PV array under Case-13 to Case-17 shading

applicability of these techniques is not feasible for the unsymmetrical sizes of PV arrays such as 3 × 4, 5 × 8, 11 × 7, 13 × 17, *etc*. However, the proposed HM technique applies and is compatible with all sizes of n × n and m × n PV arrays. To demonstrate the effectiveness of the HM technique for unsymmetrical arrays, a 3 × 5 and 4 × 3 PV array is developed as shown in Figure 22 and are tested under distinct shading conditions Case-18 and Case-19, as shown in Figure 23.

The performance of the proposed HM configuration is compared with the conventional SP, TCT, HC, and BL array configurations. The HM technique effectively disperses the shade for 3 × 5 and 4 × 3 PV arrays as shown

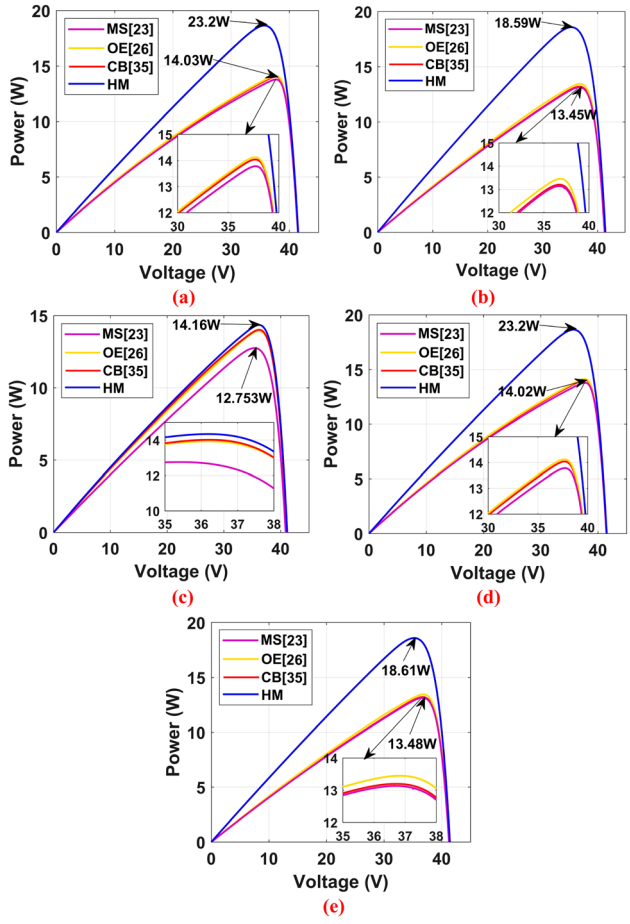

Figure 21: PV array charcteristics under (a) Case-13 to (e) Case-17

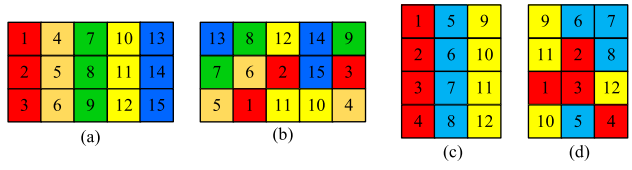

Figure 22: Original positions of (a) 3 × 5 and (c) 4 × 3 arrays, (b) and (d) corresponding rearranged matrix obtained by proposed HM

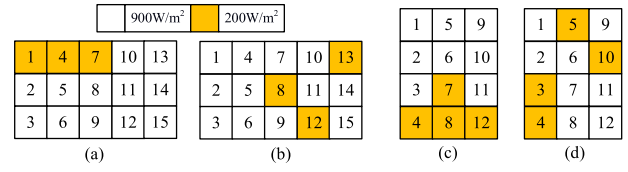

Figure 23: Shading in TCT for (a) 3 × 5 (Case-18) and (c) 4 × 3 (Case-19) PV arrays, (b) and (d) corresponding shade dispersion with HM

in Figure 23(b) and 23(d) and renders improved array PV characteristics with the highest GMP with only one MPP as shown in Figure 24(a) and 24(b). It is further

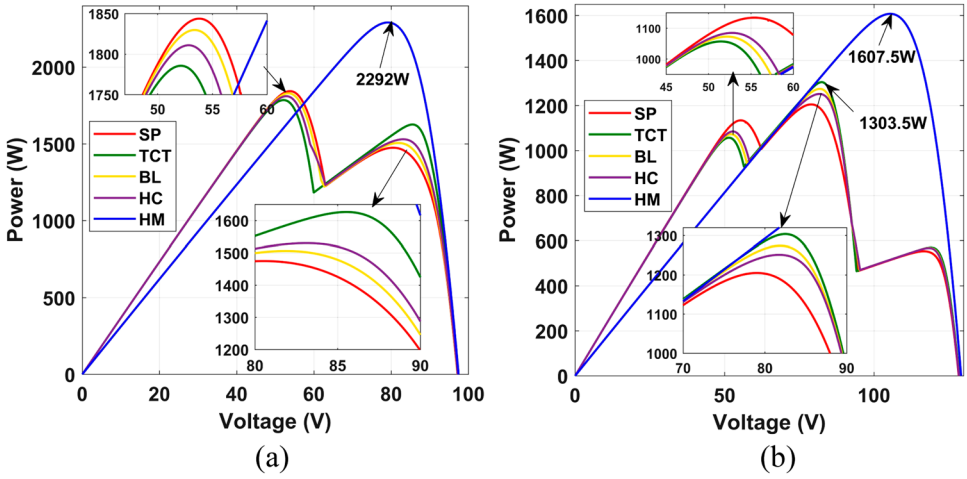

Figure 24: PV array charcteristics of (a) 3 × 5 and (c) 4 × 3 PV arrays under Case-18 and Case-19 shading

Table 7: Comparative assessment of proposed HM configuration with other notable configurations in literature

Technique	D_1	D_2	D_3	D_4	D_5	D_6	D_7	D_8	D_9
EAR [11]	H	H	L	L	H	L	H	H	H
Metaheuristic [12–15]	H	H	L	VL	H	H	H	VH	H
Sudoku [19–22]	H	M	M	M	–	M	–	M	L
MS [23]	M	M	M	M	–	M	–	M	L
OE [26]	M	VL	H	VH	H	L	–	L	L
CB [34,35]	M	M	M	H	L	M	–	M	L
OE [36]	M	VL	H	VH	H	L	–	L	L
OEP [36]	M	M	M	M	H	M	–	L	L
DTCT [38]	M	L	M	M	M	M	–	L	L
Conventional [32,33,41]	L	–	VH	H	H	L	–	L	L
Proposed	H	H	L	VL	VH	H	–	L	L

remarked that the shade dispersal ability of the proposed HM technique increases with the PV array sizing.

(D_1) Obtained GMP, (D_2) shade dispersal ability, (D_3) Row current variation, (D_4) No. of MPPs, (D_5) Compatibility, (D_6) Revenue generation, (D_7) Switches & sensors requirement, (D_8) Complexity, (D_9) Overall system cost. (L) Less, (M) Medium, (H) High, (V) Very, and (–) Nil.

5.6 Qualitative Comparative Assessment of Proposed Technique with Various State-of-the-art Techniques

A qualitative assessment of the proposed configuration with other notable configurations in literature is given in Table 7.

The proposed HM technique is compared with MS [23], CB [34,35], OE [26,36], OEP [36], and DTCT [38] techniques for various array sizes such as 9 × 9, 8 × 8 4 × 4, 3 × 5, and 4 × 3 under 19 shading cases. The application of MS technique is very limited as it is applicable to very few square matrices and not employable for many square matrices as well as unsymmetrical matrices. Hence it is not a reliable solution for PS. The existing DTCT, despite being applicable for all array sizes, yields very inferior performance under diagonal and many row-wise shading conditions (as half of the modules in the same row remains unchanged, thereby yielding suboptimal solution).

The CB technique is also not compatible with all sizes of PV array. Furthermore, this technique has the main disadvantage of generating a greater number of power peaks in the array characteristics demanding sophisticated and costly MPPT controllers as well as imposing a computational burden on MPPT system. Moreover, by employing CB, 50% of elements of a row in half of the PV array remains unchanged. Hence, if the shade occurs in any of these rows, it cannot be dispersed effectively, thus increasing the mismatch losses. The OE and OEP techniques, despite being compatible with all array sizes, have very poor shade dispersal ability as more than half of the elements in all the rows remain unchanged even after reconfiguration. This, in turn, leads to significant array mismatches and numerous MPPs, thereby imposing a burden on MPPT systems to track the GMP. Hence the reconfiguration technique based on HM is developed to overcome all the aforementioned limitations of the techniques existing in the literature.

6. CONCLUSION

Dispersing the shade over the PV array by a competent reconfiguration process mitigates the adverse impacts of partial shading. In this paper, a widely employed image encryption application-based generalized HM technique is proposed to disperse the shadow by array reconfiguration. The proposed HM configuration is extensively tested for 9 × 9, 8 × 8, 4 × 4, 3 × 5, and 4 × 3 array sizes

with seven parameters under 19 shading patterns. When compared to reconfiguration techniques based on Magic square, Chaotic Baker Map, Odd-Even, Odd-Even-Prime, Diagonal-TCT and conventional Series-Parallel and Total-Cross-Tied configurations, the proposed HM configuration evenly disperses the shade thereby equalizing the irradiance in all the rows resulting in the least mismatch losses, reduced MPPs and improved array PV characteristics. The comprehensive row current analysis of various configurations demonstrates that HM configuration renders comparatively superior performance with reduced MPPs lessening the burden on MPPT systems. The effectiveness of the proposed technique is experimentally validated in a practical scenario and tested under distinct artificial shading conditions. It is remarked that with the proposed HM configuration, there is a significant augmentation in GMP, which is in the range of (7.08–24.17)%, (8.13–25.65)%, (16.01–47.81)% for 9×9, 8×8, and 4×4 PV arrays, respectively. Besides, there is an improvement in fill factor, efficiency, performance ratio, array yield and a notable reduction in mismatch loss, row current variation, no of MPPs. Therefore, the proposed HM technique is best suitable to be executed for any array sizing under partial shading to avoid the impacts of mismatch.

7. FUTURE SCOPE

In the near future, the proposed technique can also be effectively employed in the dynamic array reconfiguration for finding the optimal switching matrix pattern. Hence, all the aforementioned setbacks associated with contemporary metaheuristic approaches and other optimization algorithms can be evaded. Further, an MPPT incorporated chaotic approach-based static and dynamic reconfiguration system for GMP tracking can also be studied for rooftop and large-rated commercial PV farms.

DISCLOSURE STATEMENT

No potential conflict of interest was reported by the author(s).

ORCID

Rayappa David Amar Raj http://orcid.org/0000-0002-5888-5513
Kanasottu Anil Naik http://orcid.org/0000-0002-3321-5097

REFERENCES

1. A. K. Gupta, Y. K. Chauhan, and T. Maity, "A new gamma scaling maximum power point tracking method for solar photovoltaic panel feeding energy storage system," *IETE. J. Res.*, Vol. 67, no. 1, pp. 15–35. DOI: 10.1080/03772063.2018.1530617.

2. P. Guerriero, and S. Daliento, "Toward a hot spot free PV module," *IEEE J. Photovolt*, Vol. 9, no. 3, pp. 796–802, 2019. DOI: 10.1109/JPHOTOV.2019.2894912.

3. Y. Mahmoud, and Z. Alqaisi, "Rule based model for power peaks of overlapped PV arrays," *IEEE Trans. Sustain. Energy*, Vol. 12, no. 2, pp. 1426–38, 2021. DOI: 10.1109/TSTE.2020.3048300.

4. B. Yang, *et al.*, "PV arrays reconfiguration for partial shading mitigation: recent advances, challenges and perspectives," *Energy Convers. Manage.*, Vol. 247, pp. 114738, 2021. DOI: 10.1016/j.enconman.2021.114738.

5. N. Kumar, S. Nema, R. K. Nema, and D. Verma, "A state-of-the-art review on conventional, soft computing, and hybrid techniques for shading mitigation in photovoltaic applications," *Int. Trans. Electr. Energy Syst*, Vol. 30, no. 9, pp. e12420, 2020. DOI:10.1002/2050-7038.12420.

6. A. I. M. Ali, H. Ramadan, and A. Mohamed, "Improved P&O MPPT algorithm with efficient open-circuit voltage estimation for two-stage grid-integrated PV system under realistic solar radiation," *Int. J. Electr. Power Energy Syst.*, Vol. 137, pp. 107805, 2022. DOI: 10.1016/j.ijepes.2021.107805.

7. D. Fares, M. Fathi, I. Shams, and S. Mekhilef, "A novel global MPPT technique based on squirrel search algorithm for PV module under partial shading conditions," *Energy Convers. Manage.*, Vol. 230, pp. 113773, 2021. DOI: 10.1016/j.enconman.2020.113773.

8. S. M. Sousa, L. S. Gusman, T. A. S. Lopes, H. A. Pereira, and J. M. S. Callegari, "MPPT algorithm in single loop current-mode control applied to dc–dc converters with input current source characteristics," *Int. J. Electr. Power Energy Syst.*, Vol. 138, pp. 107909, 2022. DOI: 10.1016/j.ijepes.2021.107909.

9. R. Celikel, M. Yilmaz, and A. Gundogdu, "A voltage scanning-based MPPT method for PV power systems under complex partial shading conditions," *Renewable Energy*, Vol. 184, pp. 361–73, 2022. DOI: 10.1016/j.renene.2021.11.098.

10. B. Yang, *et al.*, "Socio-inspired democratic political algorithm for optimal PV array reconfiguration to mitigate partial shading," *Sustain. Energy Technol. Assess*, Vol. 48, pp. 101627, 2021. DOI: 10.1016/j.seta.2021.101627.

11. K. S. Parlak, "PV array reconfiguration method under partial shading conditions," *Int. J. Electr. Power Energy Syst.*, Vol. 63, pp. 713–21, 2014. DOI:10.1016/j.ijepes.2014.06.042.

12. S. N. Deshkar, S. B. Dhale, J. S. Mukherjee, T. S. Babu, and N. Rajasekar, "Solar PV array reconfiguration under partial shading conditions for maximum power extraction using genetic algorithm," *Renewable Sustainable Energy Rev.*, Vol. 43, pp. 102–10, 2015. DOI: 10.1016/j.rser.2014.10.098.

13. T. S. Babu, J. P. Ram, T. Dragičević, M. Miyatake, F. Blaabjerg, and N. Rajasekar, "Particle swarm optimization based solar PV array reconfiguration of the maximum power extraction under partial shading conditions," *IEEE Trans. Sustain. Energy*, Vol. 9, no. 1, pp. 74–85, 2018. DOI: 10.1109/TSTE.2017.2714905.

14. D. Yousri, S. B. Thanikanti, K. Balasubramanian, A. Osama, and A. Fathy, "Multi-objective grey wolf optimizer for optimal design of switching matrix for shaded PV array dynamic reconfiguration," *IEEE. Access.*, Vol. 8, pp. 159931–46, 2020. DOI: 10.1109/ACCESS.2020.3018722.

15. D. Yousri, D. Allam, and M. B. Eteiba, "Optimal photovoltaic array reconfiguration for alleviating the partial shading influence based on a modified harris hawks optimizer," *Energy Convers. Manage.*, Vol. 206, pp. 112470, 2020. DOI: 10.1016/j.enconman.2020.112470.

16. R. Pachauri, R. Singh, A. Gehlot, R. Samakaria, and S. Choudhury, "Experimental analysis to extract maximum power from PV array reconfiguration under partial shading conditions," *Int. J. Eng. Sci. Technol.*, Vol. 22, no. 1, pp. 109–30, 2019. DOI: 10.1016/j.jestch.2017.11.013.

17. G. H. K. Varma, V. R. Barry, R. K. Jain, and D. Kumar, "An MMTES algorithm for dynamic photovoltaic array reconfiguration to enhance power output under partial shading conditions," *IET Renew. Power Gener.*, Vol. 15, no. 4, pp. 809–20, 2021. DOI:10.1049/rpg2.12070.

18. L. Bouselham, A. Rabhi, B. Hajji, and A. Mellit, "Photovoltaic array reconfiguration method based on fuzzy logic and recursive least squares: An experimental validation," *Energy*, Vol. 232, pp. 121107, 2021. DOI: 10.1016/j.energy.2021.121107.

19. B. I. Rani, G. S. Ilango, and C. Nagamani, "Enhanced power generation from PV array under partial shading conditions by shade dispersion using Su Do Ku configuration," *IEEE Trans. Sustain. Energy*, Vol. 4, no. 3, pp. 594–601, 2013. DOI: 10.1109/TSTE.2012.2230033.

20. S. G. Krishna, and T. Moger, "Optimal SuDoKu reconfiguration technique for total-cross-tied PV array to increase power output under non-uniform irradiance," *IEEE Trans. Energy Convers.*, Vol. 34, no. 4, pp. 1973–84, 2019. DOI: 10.1109/TEC.2019.2921625.

21. K. Rajani, and T. Ramesh, "Maximum power enhancement under partial shadings using modified Sudoku reconfiguration," *CSEE J. Power Energy Syst.*, Vol. 7, no. 6, pp. 1187–201, Nov. 2021. DOI: 10.17775/CSEEJPES.2020.01100.

22. S. Anjum, V. Mukherjee, and G. Mehta, "Hyper SuDoKu-based solar photovoltaic array reconfiguration for maximum power enhancement under partial shading conditions," *J. Energy Resour. Technol. ASME*, Vol. 144, no. 3, pp. 031302, 2022. DOI:10.1115/1.4051427.

23. N. Rakesh, and V. M. R. Tatabhatla, "Performance enhancement of partially shaded solar PV array using novel shade dispersion technique," *Front. Energy*, Vol. 10, pp. 227–39, 2016. DOI:10.1007/s11708-016-0405-y.

24. P. R. Satpathy, R. Sharma, and S. Jena, "A shade dispersion interconnection scheme for partially shaded modules in a solar PV array network," *Energy*, Vol. 139, pp. 350–65, 2017. DOI: 10.1016/j.energy.2017.07.161.

25. N. Belhaouas, M. S. A. Cheikh, P. Agathoklis, M. R. Oularbi, B. Amrouche, K. Sedraoui, and N. Djilali, "PV array power output maximization under partial shading using new shifted PV array arrangements," *Appl. Energy*, Vol. 187, pp. 326–37, 2017. DOI: 10.1016/j.apenergy.2016.11.038.

26. I. Nasiruddin, S. Khatoon, M. F. Jalil, and R. C. Bansal, "Shade diffusion of partial shaded PV array by using odd-even structure," *Sol. Energy*, Vol. 181, pp. 519–29, 2019. DOI: 10.1016/j.solener.2019.01.076.

27. B. Dhanalakshmi, and N. Rajasekar, "A novel Competence square based PV array reconfiguration technique for solar PV maximum power extraction," *Energy Convers. Manage.*, Vol. 174, pp. 897–912, 2018. DOI: 10.1016/j.enconman.2018.08.077.

28. P. R. Satpathy, and R. Sharma, "Power loss reduction in partially shaded PV arrays by a static SDP technique," *Energy*, Vol. 156, pp. 569–85, 2018. DOI: 10.1016/j.energy.2018.05.131.

29. B. Dhanalakshmi, and N. Rajasekar, "Dominance square based array reconfiguration scheme for power loss reduction in solar PhotoVoltaic (PV) systems," *Energy Convers. Manage.*, Vol. 156, pp. 84–102, 2018. DOI: 10.1016/j.enconman.2017.10.080.

30. P. R. Satpathy, and R. Sharma, "Power and mismatch losses mitigation by a fixed electrical reconfiguration technique for partially shaded photovoltaic arrays," *Energy Convers. Manage.*, Vol. 192, pp. 52–70, 2019. DOI: 10.1016/j.enconman.2019.04.039.

31. M. S. S. Nihanth, J. P. Ram, D. S. Pillai, A. M. Y. M. Ghias, A. Garg, and N. Rajasekar, "Enhanced power production in PV arrays using a new skyscraper puzzle based one-time reconfiguration procedure under partial shade conditions (PSCs)," *Sol. Energy*, Vol. 194, pp. 209–24, 2019. DOI: 10.1016/j.solener.2019.10.020.

32. A. A. Desai, and S. Mikkili, "Novel hybrid PV configurations to enhance the output power and efficiency by minimising the number of peaks and mismatching loss," *IETE. J. Res.* 2021. DOI: 10.1080/03772063.2021.1943012.

33. P. K. Bonthagorla, and S. Mikkili, "A novel fixed PV array configuration for harvesting maximum power from shaded modules by reducing the number of cross-ties," *IEEE. J. Emerg. Sel. Top. Power. Electron.*, Vol. 9, no. 2, pp. 2109–21, 2021. DOI: 10.1109/JESTPE.2020.2979632.

34. V. M. R. Tatabhatla, A. Agarwal, and T. Kanumuri, "Improved power generation by dispersing the uniform and non-uniform partial shades in solar photovoltaic array," *Energy Convers. Manage.*, Vol. 197, pp. 111825, 2019. DOI:10.1016/j.enconman.2019.111825.

35. V. M. R. Tatabhatla, A. Agarwal, and T. Kanumuri, "A generalized chaotic baker map configuration for reducing the power loss under shading conditions," *Electr. Eng.*, Vol. 102, pp. 2227–44. DOI:10.1007/s00202-020-01016-4.

36. S. S. Reddy, and C. Yammani, "Odd-even-prime pattern for PV array to increase power output under partial shading conditions," *Energy*, Vol. 213, pp. 118780, 2020. DOI:10.1016/j.energy.2020.118780.

37. R. Venkateswari, and N. Rajasekar, "Power enhancement of PV system via physical array reconfiguration based Lo Shu technique," *Energy Convers. Manage.*, Vol. 215, pp. 112885, 2020. DOI:10.1016/j.enconman.2020.112885.

38. V. P. Madhanmohan, M. Nandakumar, and A. Saleem, "Enhanced performance of partially shaded photovoltaic arrays using diagonally dispersed total cross tied configuration," *Energy Sources Part A*, DOI: 10.1080/15567036.2020.1826008.

39. V. C. Chavan, and S. Mikkili, "Effect of PV array positioning on mismatch and wiring losses in static array reconfiguration," *IETE. J. Res.* 2021. DOI: 10.1080/03772063.2021.1945957.

40. N. Rakesh, S. Subramaniam, B. Natarajan, and M. Udugula, "A non-puzzle based interconnection scheme for energy savings and income generation from partially shaded photovoltaic modules," *Energy Sources Part A* (2022. DOI: 10.1080/15567036.2022.2029973.

41. G. H. K. Varma, V. R. Barry, and R. K. Jain, "A novel magic square based physical reconfiguration for power enhancement in larger size photovoltaic array," *IETE. J. Res.* 2021. DOI: 10.1080/03772063.2021.1944333.

42. W. Shinong, M. Qianlong, X. Jie, G. Yuan, and L. Shilin, "An improved mathematical model of photovoltaic cells based on datasheet information," *Sol. Energy*, Vol. 199, pp. 437–46, 2020. DOI:10.1016/j.solener.2020.02.046.

43. X. Kang, and R. Tao, "Color image encryption using pixel scrambling operator and reality-preserving MPFRHT," *IEEE Trans. Circuits Syst. Video Technol.*, Vol. 29, no. 7, pp. 1919–32, 2019.

44. T. Li, B. Du, and X. Liang, "Image encryption algorithm based on logistic and two-dimensional Lorenz," *IEEE. Access.*, Vol. 8, pp. 13792–805, 2020.

45. M. Henon, "A two-dimensional mapping with a strange attractor," *Commun. Math. Phys.*, Vol. 50, pp. 69–77, 1976.

46. P. Ping, Y. Mao, X. Lv, F. Xu, and G. Xu, "An image scrambling algorithm using discrete Henon map," *Int. Conf. Inf. Autom*, pp. 429–32, 2015.

APPENDIX

Table A1: Specifications of PV panel

Parameter	Specification	
	Simulation	Experimental
Maximum power, P_{MPP}	200 W	3 W
Open circuit voltage, V_{oc}	32.9 V	10.8 V
Short circuit current, I_{sc}	8.21 A	0.38 A
Maximum power voltage, V_{MPP}	26.3 V	9.01 V
Maximum power current, I_{MPP}	7.61 A	0.34 A

AUTHORS

Rayappa David Amar Raj is a research scholar at the National Institute of Technology, Warangal, India. He holds a master's degree from the National Institute of Technology, Agartala, India. His areas of research include solar PV array reconfiguration, solar energy systems, power systems, image encryption techniques, and faults in a grid-connected solar photovoltaic system.

Corresponding author. Email: dtcdavid2k15@gmail.com

Kanasottu Anil Naik has received PhD from the Indian Institute of Technology Roorkee in 2018. He has obtained M.Tech and B.Tech from the National Institute of Technology Hamirpur and JNTU Hyderabad, respectively. He is currently working as an assistant professor at the National Institute of Technology, Warangal. His research interests include wind energy systems, micro-grid stability, and DSP techniques application in power system.

Email: anilnaik205@nitw.ac.in